VORTEX2 observations and data assimilation experiments of the 18 May 2010 Dumas, Texas supercell

Patrick S. Skinner,* Christopher C. Weiss,
Texas Tech University
Louis J. Wicker, Corey K Potvin
NOAA/National Severe Storms Laboratory,
and David C. Dowell
NOAA/Earth System Research Laboratory

1. Introduction

On 18 May 2010, a high-precipitation, weakly-tornadic supercell in the Texas Panhandle was intercepted by instruments participating in the second Verification of the Origin of Rotation in Tornadoes Experiment (VORTEX2) (Wurman et al. 2012). A fifteen minute period during the pretornadic phase of the supercell was well-sampled by several mobile Doppler radars including a dual-Doppler deployment by two Ka-band radars operated by Texas Tech University (TTUKa) (Weiss et al. 2009) and the X-band MWR-05XP radar operated by the University of Oklahoma and the Naval Postgraduate School (Bluestein et al. 2010). Analysis of near-surface dual-Doppler syntheses with high spatial resolution from the TTUKa radars and volumetric single-Doppler MWR-05XP data with high temporal resolution reveals the development and decay of a low-level mesocyclone coupled with the succession of four internal rear-flank downdraft (RFD) surges over the period of interest (2250 - 2305 UTC, all times hereafter are given in UTC) (Skinner et al. 2012).

While examination of TTUKa and MWR-05XP data reveals the rapid evolution of small-scale features within the Dumas supercell and allows for a qualitative interpretation of the dynamics influencing storm evolution, a four-dimensional representation of the thermodynamic and kinematic properties within the Dumas supercell is required for a quantitative analysis. In an effort to produce a representative four-dimensional analysis of the Dumas supercell, a series of ensemble Kalman filter (EnKF) data assimilation experiments have been produced (Marquis et al. 2012; Tanamachi et al. 2012; Dowell et al. 2012) by assimilating C-band mobile Doppler radar from the Shared Mobile Atmospheric and Teaching Radar (SMART-R) (Biggerstaff et al. 2005) and KAMA WSR-88D data. Preliminary results of the EnKF experiments will be presented herein and compared to the independent TTUKa and MWR-05XP observations to assess their ability to reproduce the small-scale and rapidly-evolving low-level mesocyclone and internal RFD surges observed within the Dumas supercell.

Corresponding author address: Patrick Skinner, Texas Tech University, Wind Science and Engineering Research Center, 10^{th} and Akron, Lubbock, TX 79409.
E-mail: patrick.skinner@ttu.edu

2. Methodology

a. *Mobile Doppler radar quality assurance and analysis*

Mobile radar data collected on 18 May have been quality assured using the SOLOII and DORADE Radar Editing Algorithms, Detection, Extraction and Retrieval (DREADER) software available from the National Center for Atmospheric Research and the National Oceanic and Atmospheric Administration's Earth System Research Laboratory, respectively. Radar data are reoriented to earth-relative coordinates by matching clutter patterns to the location of known structures, then thresholded to remove incoherent returns, have regions of ground clutter manually removed and aliased radial velocities unfolded. Additional quality assurance is required for issues unique to individual radar platforms. TTUKa data are despeckled using DREADER to remove areas of speckling introduced by improper dealiasing in scans utilizing an interleaved dual-pulse repetition frequency (Jorgensen et al. 2000). As the MWR-05XP platform is not equipped with a hydraulic leveling system, an attempt has been made to quantify the spatial errors in the data resulting from variation of the pitch and roll angles of the platform. A data horizon is not observed in the 1° elevation scans of the MWR-05XP, which suggests that roll and pitch errors are less than 1°, which is further supported by photographs of the deployment site. Adopting 1° as the maximum possible offset in the MWR-05XP data and 20 km as the maximum range to relevant storm features on 18 May results in horizontal(vertical) displacement errors of less than 100(400) m in magnitude (French 2012), which will minimally impact a qualitative analysis of storm features.

Mobile radar data are objectively analyzed to a Cartesian grid using a two-pass Barnes analysis according to the recommendations of Majcen et al. (2008). The Barnes smoothing parameter (κ) is defined as $(1.33\mu)^2$ where μ is the coarsest gate spacing included in the analysis in kilometers (Pauley and Wu 1990; Trapp and Doswell 2000). Different smoothing parameters are employed depending on the platform being analyzed and the type of analysis being performed. For example, 0.0° elevation angle TTUKa data are interpolated to a 20 x 20 km domain with 50 m grid spacing for single-Doppler analysis and a 7 x 7 km grid with 25 m grid spacing for dual-Doppler synthesis as the smaller grid encompassed the entirety of the dual-Doppler lobe. Volumetric MWR-05XP data are interpreted to a 20 x 20 x 12.5 km domain with 250 m grid spacing[1], and SMART-R1 data are interpolated with 1 km grid spacing to the EnKF experiment domain.

Rotation in single-Doppler MWR-05XP data is approximated using the azimuthal wind shear, which is calculated as $\partial V_r/\partial\phi(r^{-1})$ where V_r is the radial velocity, ϕ is the azimuth of the radar beam and r is the range from the radar. Azimuthal wind shear will be equal to twice the vertical vorticity for regions of near solid-body rotation and a recent study combining single- and dual-Doppler data found that the two fields evolved similarly (Markowski et al. 2012).

b. *Numerical model and ensemble Kalman filter specifications*

Simulations of the Dumas supercell are produced using the National Severe Storms Laboratory Collaborative Model for Multiscale Atmospheric Simulation (NCOMMAS) (Wicker and Skamarock 2002; Coniglio et al. 2006). Simulations are initialized in a horizontally homogeneous base state with potential temperature and mixing ratio values based on a mobile sounding launched by VORTEX2 at 2152 approximately 20 km south of Dumas and modified near the surface towards observations in subsequent soundings launched in the near-inflow of the Dumas supercell. The base state wind profile is taken from the 0000 KAMA sounding. Simulations are run on a 100 x 100 x 20 km grid with uniform 500(250) m horizontal(vertical) grid spacing and a 2 s model time step. The Lin et al. (1983) microphysical parameterization is utilized with rain(hail/graupel) intercept parameters of 8.0 x 10^6(4.0 x 10^4) m^{-4} and a hail density of 900 kg m^{-3} (Gilmore et al. 2004).

Prior to data assimilation, convection is initiated in the 36 member ensemble by introducing random thermodynamic perturbations across the region of reflectivity encompassed by the Dumas supercell. Base state wind profiles are perturbed with sinusoidal noise with a 0 m s^{-1} mean and a standard deviation of 2 m s^{-1} at the lowest grid level linearly increasing to 6 m s^{-1} at the top of the domain to enhance ensemble spread. Data assimilation of KAMA WSR-88D and SMART-R1 data using an ensemble square root filter (EnSRF) (Dowell and Wicker 2009) begins 20 minutes into the simulations (2220) and continues for 45 minutes with 2.5 minute assimilation cycles. Radial velocities from KAMA are objectively analyzed to a 2 km grid using a Cressman scheme and assimilated with 1 km objectively analyzed SMART-R1 radial velocities. Two missing volumes of SMART-R1 data between 2248 and 2254 are replaced by interpolation of surrounding volumes of SMART-R1 data according to the mean storm motion. Radar reflectivity values from KAMA are assimilated as well, with 0 dBZ substituted for reflectivities less than 20 dBZ to suppress spurious convection. Reflectivity values are additionally prevented from updating potential temperature values to limit their effect on the development of the low-level cold pool (Dowell et al. 2011). Observation error standard deviations of 2 m s^{-1}(2 dBZ) are prescribed to the radial velocity(radar reflectivity) observations and a localization factor based on Gaspari and Cohn (1999) is applied. Additive noise with standard deviations of 1 m s^{-1}, 1 m s^{-1}, 1 K and 1 K is added to the simulated lateral wind, meridional wind, potential temperature, and dewpoint temperature fields in regions of high simulated reflectivity to promote ensemble spread (Dowell and Wicker 2009).

3. Results

a. *Overview of observational findings*

Near-surface TTUKa single- and dual-Doppler data reveal a series of four compact regions of enhanced momentum and associated convergence boundaries within the broad-scale RFD (Figs. 1, 2).

[1]TTUKa single-Doppler data are additionally interpreted with 250 m grid spacing and MWR-05XP data with 500 x 500 x 250 m grid spacing to facilitate visualization and comparison to EnKF output (Figs. 3, 6, 7)

These RFD "surges" have been regularly observed by mobile Doppler radar and in situ probes over the past decade and have been shown to contribute to tornado genesis (Kosiba et al. 2012; Lee et al. 2012), maintenance (Marquis et al. 2012) and demise (Marquis et al. 2012; Lee et al. 2012). RFD surges observed by the TTUKa radars in the Dumas supercell may be grouped into two categories: a relatively long-lived surge (A) observed over roughly the first half of the period of interest (Figs. 1b - 1d) and three additional surges (B, C, D) that develop and merge in rapid succession over the second half of the analysis period (Figs. 1c - 2h). Surges B, C and D are oriented differently than surge A, and additionally exhibit stronger straight line wind speeds and stronger cyclonic rotation north of the apex of the leading surge, with a brief, intense near-surface vortex occurring north of the apex of surge D (Figs. 1, 2).

The development of surges B, C and D coincides with intensification of a low-level mesocyclone in MWR-05XP data distinct from the midlevel mesocyclone (Figs. 3 - 5). This low-level mesocyclone intensifies during a period where it is minimally displaced from a relatively intense midlevel mesocyclone (Fig. 4) and surges B, C and D are first observed following intensification of azimuthal wind shear near the surface to values greater than those aloft. This evolution is similar to low-level mesocyclogenesis and occlusion downdraft development driven by vertical perturbation pressure gradient forces in numerical modeling studies (Wicker and Wilhelmson 1995; Adlerman et al. 1999). An intense and minimally displaced midlevel mesocyclone would trigger an upward directed perturbation pressure gradient force on the low levels, leading to acceleration of the low-level vertical wind and enhanced tilting and stretching of vertical vorticity. As this low-level vertical vorticity intensifies to values greater than those aloft, a second, downward-directed perturbation pressure gradient force will be induced, triggering an occlusion downdraft. The final three RFD surges observed during the period of interest are hypothesized to be the surface manifestation of an occlusion downdraft as they develop along the western periphery of the low-level mesocyclone during a period when rotation near the surface was greater than that aloft (Figs. 4, 5).

At its most intense, the low-level mesocyclone observed in the Dumas supercell bears a resemblance to the early stages of the 5 June 2009 low-level mesocyclone that would go on to produce the Goshen County, Wyoming tornado (Markowski et al. 2012). However, rather than expanding upwards through the depth of the troposphere and eventually producing a tornado, the low-level mesocyclone of the Dumas supercell never extends beyond 2 km in depth and rapidly decays near the end of the period of interest. This implies that convergence along RFD gust fronts and upward-directed perturbation pressure gradient forces within the Dumas supercell were insufficient to lift air parcels exhibiting moderate buoyancy deficits (Skinner et al. 2012) within the RFD and RFD surges to their level of free convection and leading to tornadogenesis failure.

b. *Representativeness of EnKF analyses*

In order to perform a quantitative analysis of the hypotheses presented above, a representative simulation of the Dumas supercell must be constructed. Of particular interest is the ability of the simulation to capture the proper location and evolution of the rapidly-evolving low-level mesocyclone and internal RFD surges in the Dumas supercell.

Azimuthal wind shear values in MWR-05XP data are compared with posterior ensemble mean vertical vorticity to assess the ability of the EnKF to capture the position and evolution of the low-level mesocyclone (Fig. 6). Initial development of the low-level mesocyclone in the EnKF analysis is displaced to the east of observations and is associated with convergence across the broad-scale RFD gust front rather than the gust front of internal surge A (Fig. 7). However, a second low-level mesocyclone does develop in a location consistent with observations by 2300 (Fig. 6). This secondary low-level mesocyclone evolves similarly in the EnKF to observations through the remainder of the period of interest, however the erroneous development of the low-level mesocyclone continues through the period as well and by 2305 cyclic mesocyclogenesis has occurred in the model. MWR-05XP observations do show signs of cyclic mesocyclogenesis during the latter portions of the period of interest, but they are less pronounced than in the EnKF analyses.

The spurious development of the low-level mesocyclone across the broad-scale RFD gust front occurs due to stronger than observed wind speeds across the gust front in EnKF analyses (Fig. 7). Additionally, surge A is underrepresented in the EnKF output, resulting in the initial lack of low-level mesocyclone development within the broad-scale RFD. However, surges B-D are well-represented in the EnKF analysis in a similar location to observations and with a similar wind speed magnitude. Though surges B-D are represented as single RFD surge in the EnKF analysis, the relatively coarse spatial and temporal resolution of the model compared to TTUKa observations is likely insufficient to resolve the evolution of the multiple surges.

Errors in the representation of the low-level mesocyclone and RFD surges in EnKF output are likely exacerbated by the two missing volumes of SMART-R data from 2248 - 2254.

4. Summary and Future Work

Mobile Doppler radar observations and preliminary EnKF analyses of a 15 minute period during the pretornadic phase of the Dumas supercell have been presented. The devolopment and evolution of four internal RFD surges coincides with the intensification and decay of a low-level mesocyclone distinct from midlevel rotation. The low-level mesocyclone develops and intensifies in a region of inferred upward-directed perturbation pressure gradient force north of the apex of the leading RFD surge gust front, then decays as it becomes displaced vertically and horizontally from the midlevel mesocyclone (Fig. 4). The intensification of the low-level mesocyclone appears to induce a second, downward-directed perturbation pressure gradient force that drives an occlusion downdraft which manifests itself at the surface as RFD surges B-D. Convergence along internal RFD surge gust fronts and upward-directed perturbation pressure gradient forcing was either too weak or not sustained for a long enough period to allow the low-level mesocyclone to expand through the depth of the troposphere, resulting in tornadogenesis failure.

Initial EnKF data assimilation experiments of the Dumas supercell capture the development of RFD surges B-D and the latter evolution of the low-level mesocyclone well. However, surge A is poorly represented and spurious low-level mesocyclone development occurs across the broad-scale RFD gust front, leading to premature cyclic mesocyclogenesis. Errors in the EnKF analyses are likely influenced by two missing volumes of SMART-R1 data early in the period of interest. These volumes have been recovered and assimilation of the full SMART-R1 dataset, as well as additionally assimilating radial velocity data from a Doppler-on-Wheels deployment will likely result in a better representation of the low-level mesocyclone and internal RFD surges in the EnKF analyses, permitting a quantitative analysis of the forcing terms in the vertical momentum equation acting upon the low-levels of the Dumas supercell to be undertaken.

Acknowledgments.

This study was supported by National Science Foundation Grant AGS-0964088. The authors wish to thank Drs. Michael French, Howard Bluestein, Paul Markowski and Yvette Richardson for their collaboration on the observational aspects of this study and for making available the MWR-05XP and mobile mesonet data. Dr. Ivan PopStefanija, Dr. Robert Bluth, Dr. John Schroeder, Jerry Guynes, Scott Gunter, Anthony Reinhart and Amanda Thibault are acknowledged for their assistance with MWR-05XP and TTUKa data collection. The author's benefited from software provided by Drs. Curtis Alexander, Brian Hirth and Sylvie Lorsolo and conversations with Dr. Jim Marquis, Anthony Reinhart and Daniel Betten. Dr. Matthew Parker, Dr. George Bryan and Dr. Michael Biggerstaff are thanked for providing mobile sounding and SMART-R data of the Dumas supercell, which was generously hosted by NCAR/EOL under sponsorship of the National Science Foundation.

REFERENCES

Adlerman, E. J., K. K. Droegemeier, and R. Davies-Jones, 1999: A numerical simulation of cyclic mesocyclogenesis. *J. Atmos. Sci.*, **56**, 2045–2069.

Biggerstaff, M. I., et al., 2005: The Shared Mobile Atmospheric Research and Teaching Radar: A collaboration to enhance research and teaching. *Bull. Amer. Meteor. Soc.*, **86**, 1263–1274.

Bluestein, H. B., M. M. French, I. PopStefanija, R. T. Bluth, and J. B. Knorr, 2010: A mobile, phased-array Doppler radar for the study of severe convective storms. *Bull. Amer. Meteor. Soc.*, **91**, 579–600.

Coniglio, M. C., D. J. Stensrud, and L. J. Wicker, 2006: Effects of upper-level shear on the structure and maintenance of strong quasi-linear mesoscale convective systems. *J. Atmos. Sci.*, **63**, 1231–1252.

Dowell, D. C., C. C. Weiss, A. E. Reinhart, and P. S. Skinner, 2012: Baroclinity and mesocyclogenesis in a simulation of the VORTEX2 18 May 2010 Dumas, Texas supercell. *Preprints, 26th Conf. Severe Local Storms*, Nashville, TN, Amer. Meteor. Soc., 13.5.

Dowell, D. C. and L. J. Wicker, 2009: Additive noise for storm-scale ensemble data assimilation. *J. Atmos. Oceanic Technol.*, **26**, 911–927.

Dowell, D. C., L. J. Wicker, and C. Snyder, 2011: Ensemble Kalman filter assimilation of radar observations of the 8 May 2003 Oklahoma City supercell: Influences of reflectivity observations on storm-scale analyses. *Mon. Wea. Rev.*, **139**, 272–294.

French, M. M., 2012: Mobile, phased-array, Doppler radar observations of tornadoes at X band. Ph.D. thesis, University of Oklahoma, 322 pp., [Available from School of Meteorology, University of Oklahoma, 120 David L. Boren Blvd. Suite 5900, Norman, OK 73072.].

Gaspari, G. and S. E. Cohn, 1999: Construction of correlation functions in two and three dimensions. *Quart. J. Roy. Meteor. Soc.*, **125**, 723–757.

Gilmore, M. S., J. M. Straka, and E. N. Rasmussen, 2004: Precipitation and evolution sensitivity in simulated deep convective storms: Comparisons between liquid-only and simple ice and liquid phase microphysics. *Mon. Wea. Rev.*, **132**, 1897–1916.

Jorgensen, D. P., T. R. Shepherd, and A. S. Goldstein, 2000: A dual-pulse repitition frequency scheme for mitigating velocity ambiguities of the NOAA P-3 airborne Doppler radar. *J. Atmos. Oceanic Technol.*, **17**, 585–594.

Kosiba, K., J. Wurman, Y. Richardson, P. Markowski, P. Robinson, and J. Marquis, 2012: Genesis of the Goshen County, Wyoming tornado on 05 June 2009 during VORTEX2. *Mon. Wea. Rev., in press.*

Lee, B. D., C. A. Finley, and C. D. Karstens, 2012: The Bowdle, South Dakota, cyclic tornadic supercell of 22 May 2010: Surface analysis of rear-flank downdraft evolution and multiple internal surges. *Mon. Wea. Rev.*, **139**, 3419–3441.

Lin, Y.-L., R. D. Farley, and H. D. Orville, 1983: Bulk parameterization of the snow field in a cloud model. *J. Climate Appl. Meteor.*, **22**, 1065–1092.

Majcen, M., P. Markowski, Y. Richardson, D. Dowell, and J. Wurman, 2008: Multipass objective analysis of Doppler radar data. *J. Atmos. Oceanic Technol.*, **25**, 1845–1858.

Markowski, P. M., et al., 2012: The pretornadic phase of the Goshen County, Wyoming supercell of 5 June 2009 intercepted by VORTEX2. part I: Evolution of kinematic and surface thermodynamic fields. *Mon. Wea. Rev.*, **140**, 2887–2915.

Marquis, J., Y. P. Richardson, P. M. Markowski, D. C. Dowell, and J. Wurman, 2012: Tornado maintenance investigated with high-resolution dual-Doppler and EnKF analysis. *Mon. Wea. Rev.*, **140**, 3–27.

Pauley, P. M. and X. Wu, 1990: The theoretical, discrete, and actual response of the barnes objective analysis scheme for one- and two-dimensional fields. *Mon. Wea. Rev.*, **130**, 1692–1721.

Skinner, P. S., C. C. Weiss, M. M. French, H. B. Bluestein, P. M. Markowski, and Y. P. Richardson, 2012: VORTEX2 observations of multiple internal rear-flank downdraft momentum surges associated with a low-level mesocyclone cycle in the 18 May 2010 Dumas, Texas supercell. *Mon. Wea. Rev., In Preparation.*

Tanamachi, R. L., L. J. Wicker, D. C. Dowell, H. B. Bluestein, D. T. Dawson, and M. Xue, 2012: EnKF assimilation of high-resolution, mobile Doppler radar data of the 4 May 2007 Greensburg, Kansas supercell into a numerical cloud model. *Mon. Wea. Rev., In Press.*

Trapp, R. J. and C. A. Doswell, 2000: Radar data objective analysis. *J. Atmos. Oceanic Technol.*, **17**, 105–120.

Weiss, C. C., J. L. Schroeder, J. Guynes, P. S. Skinner, and J. Beck, 2009: The TTUKa mobile Doppler radar: Coordinated radar and in situ measurements of supercell thunderstorms during Project VORTEX2. *Preprints, 34th Conf. on Radar Meteorology*, Williamsport, VA, Amer. Meteor. Soc., 11B.2.

Wicker, L. J. and W. C. Skamarock, 2002: Time-splitting methods for elastic models using forward time schemes. *Mon. Wea. Rev.*, **130**, 2088–2097.

Wicker, L. J. and R. B. Wilhelmson, 1995: Simulation and analysis of tornado development and decay within a three-dimensional supercell thunderstorm. *J. Atmos. Sci.*, **52**, 2675–2703.

Wurman, J., D. Dowell, Y. Richardson, P. Markowski, E. Rasmussen, D. Burgess, L. Wicker, and H. B. Bluestein, 2012: The second verification of the origin of rotation in tornadoes experiment: VORTEX2. *Bull. Amer. Meteor. Soc.*, **93**, 1147–1170.

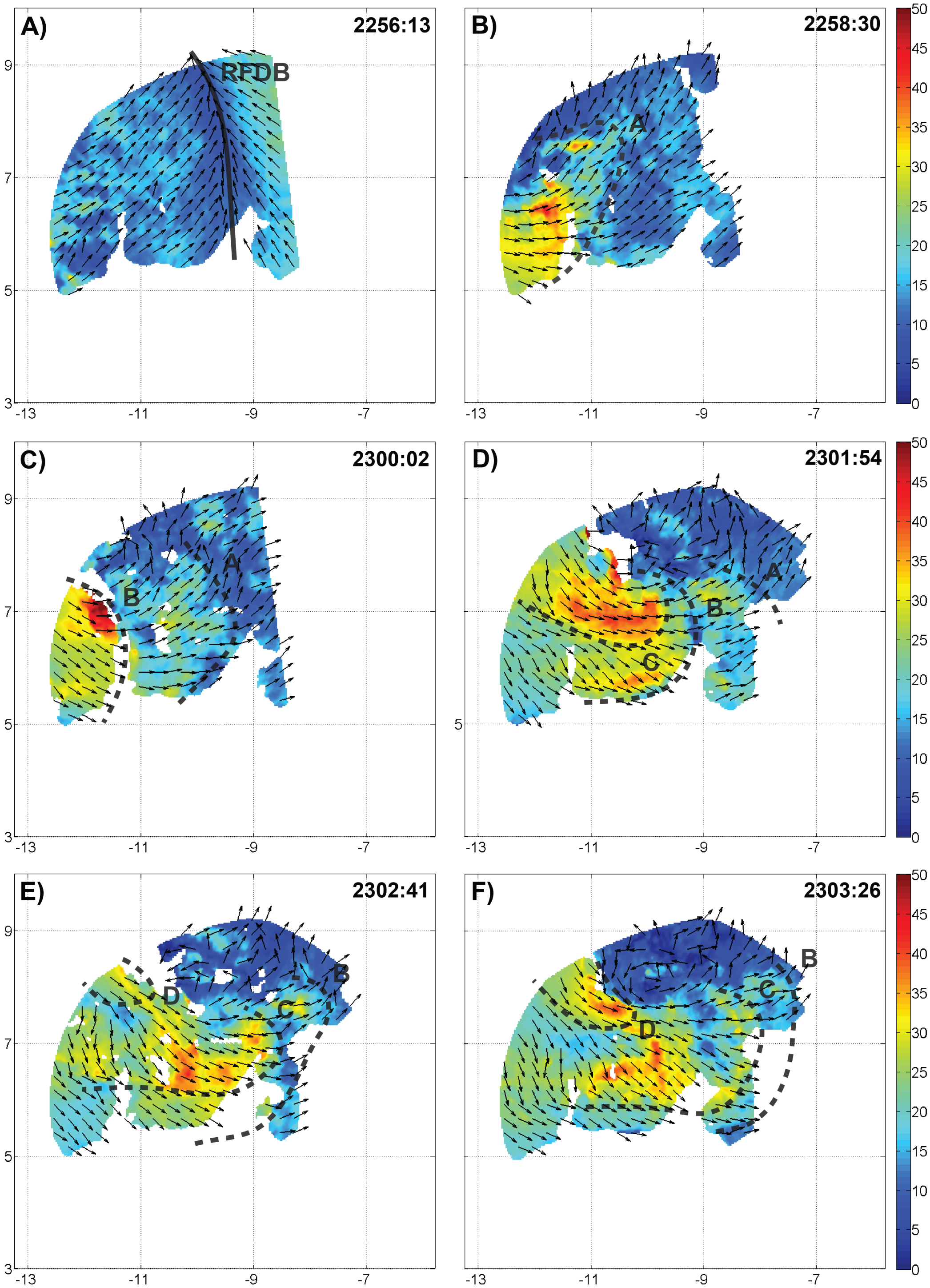

A)
2256:13
RFDB
B)
2258:30
A
C)
2300:02
B
A
D)
2301:54
A
B
C
E)
2302:41
D
C
B
F)
2303:26
B
C
D

Fig. 1.

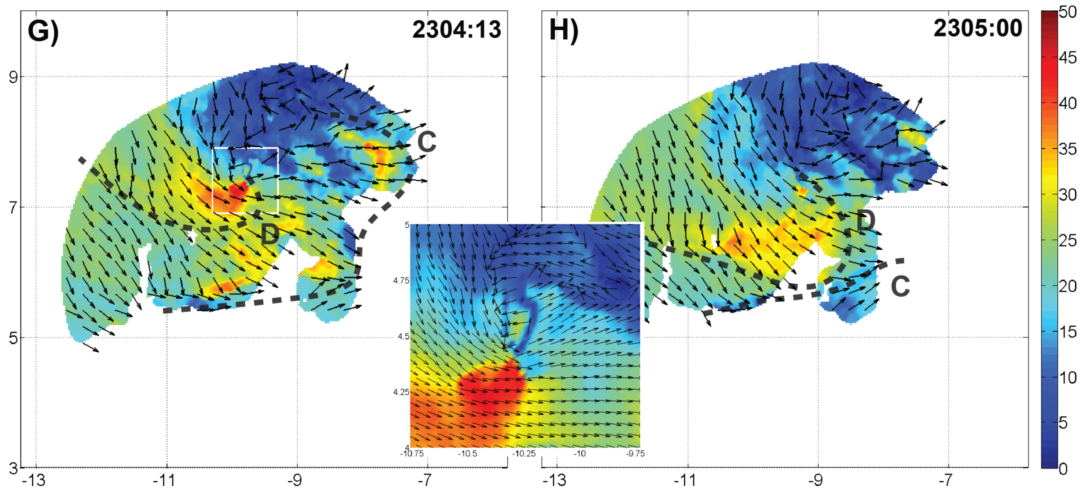

Fig. 2. TTUKa 0.0° elevation dual-Doppler analyses of ground-relative wind speed (m s^{-1}) and wind direction vectors plotted every 8th grid point at (A) 2256:13, (B) 2258:30, (C) 2300:02, (D) 2301:54, (E) 2302:41, (F) 2303:26, (G) 2304:13 and (H) 2305:00. Subjectively analyzed positions of the primary RFD gust front (bold line) and internal RFD surge gust fronts (dashed lines) are indicated. The white square in panel G bounds the region of the figure inset, which is a close-up of the dual-Doppler analysis around the intense near-surface vortex observed at 2304:13. Inset colorbar is the same as the other panels and wind direction vectors are plotted every 2nd grid point. Horizontal grid is distance in km from location of the MWR-05XP.

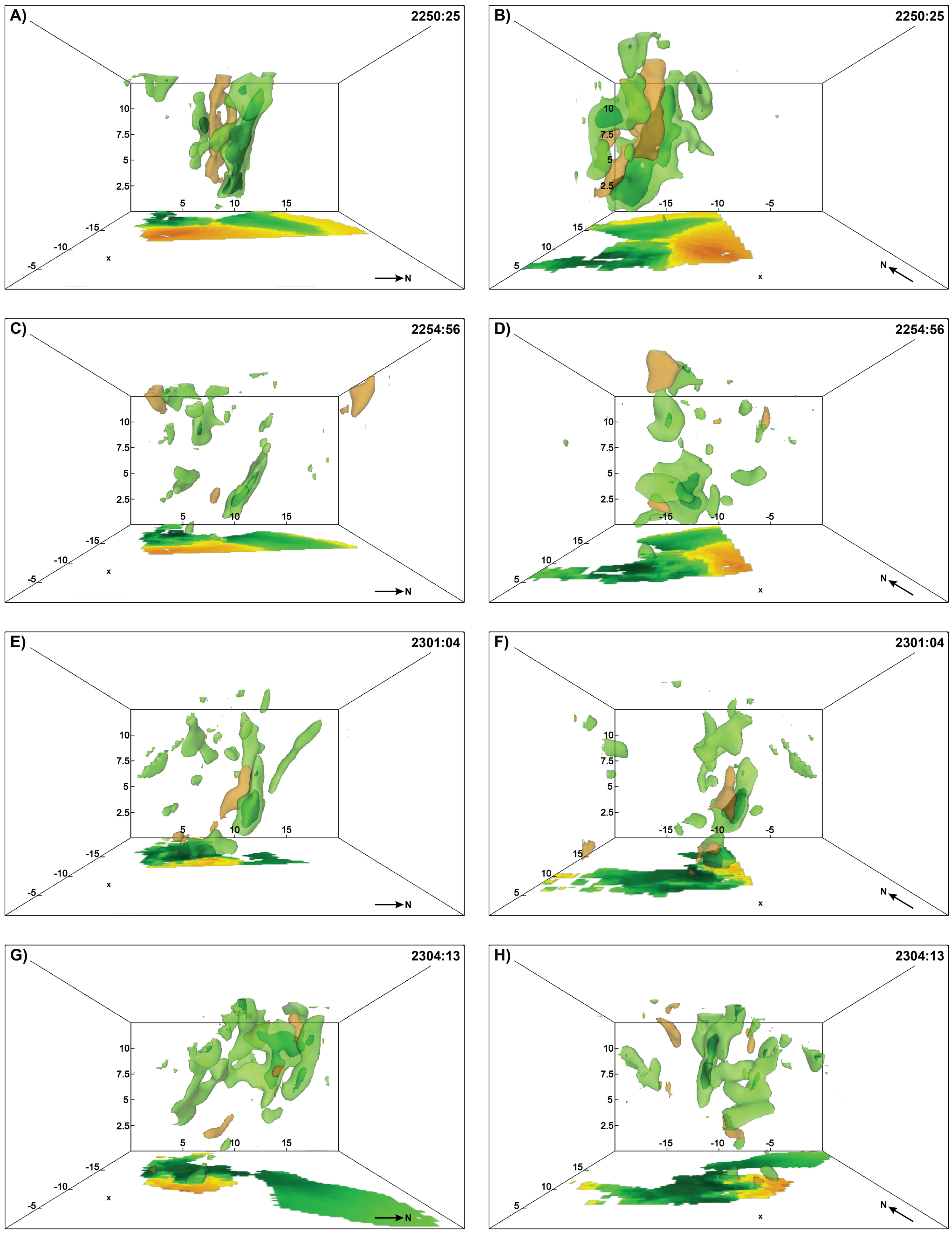

FIG. 3. Three-dimensional isosurfaces of MWR-05XP objectively analyzed azimuthal wind shear (s^{-1}) for (A, B) 2250:25, (C, D) 2254:56, (E, F) 2301:04 and (G, H) 2304:13. Viewing perspective is from the east for panels A, C, E and G and from the south for panels B, D, F, and H. Isosurfaces of cyclonic azimuthal shear values of 0.0125(0.02) are plotted in light(dark) green and isosurfaces of anticyclonic azimuthal wind shear values of -0.0125 are plotted in brown. Objectively analyzed TTUKa-2 0.0° elevation radial velocity (m s^{-1}) with 250 m grid spacing at the nearest available time to the MWR-05XP volume is underlain. The times of the TTUKa-2 radial velocity scans vary with the times of the MWR-05XP volume by less than 30 s. Grid labels are given in km from MWR-05XP location and “x” represents the location of TTUKa-2.

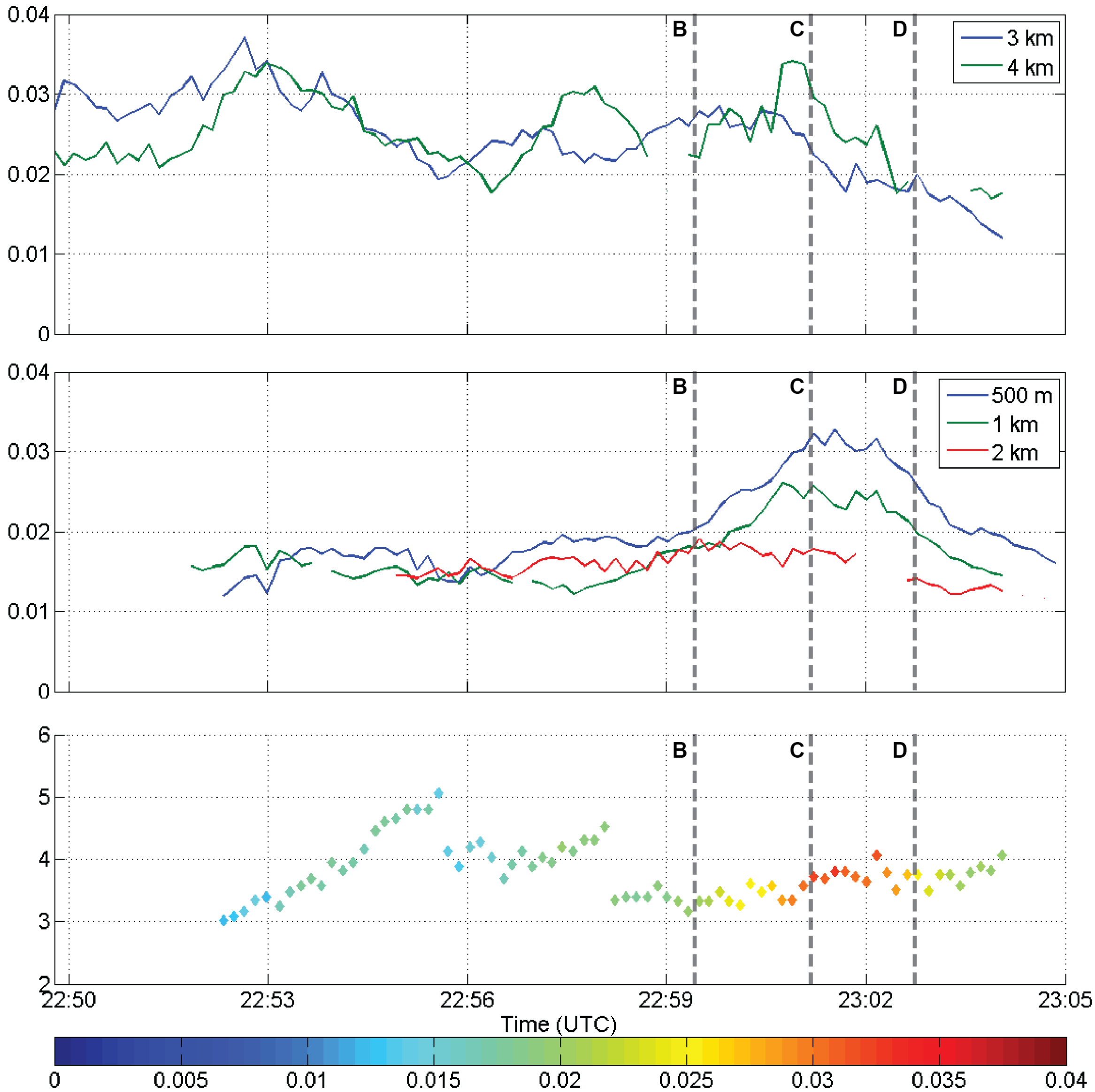

FIG. 4. Time-series of maximum cyclonic azimuthal wind shear (s^{-1}) in objectively analyzed MWR-05XP data for grid levels of (A) 3 km, 4km, (B) 500 m, 1 km and 2 km AGL. Distance (km) between maximum cyclonic azimuthal wind shear at 3 km and 500 m is plotted in C. Periods of missing data represent times when the maximum cyclonic azimuthal wind shear at a given level was not associated with the primary low- and midlevel mesocyclones within the Dumas supercell. Data points in (C) are color coded according the maximum cyclonic azimuthal wind shear at 500m. Dashed lines indicate times when internal surges B, C and D were first observed in TTUKa data.

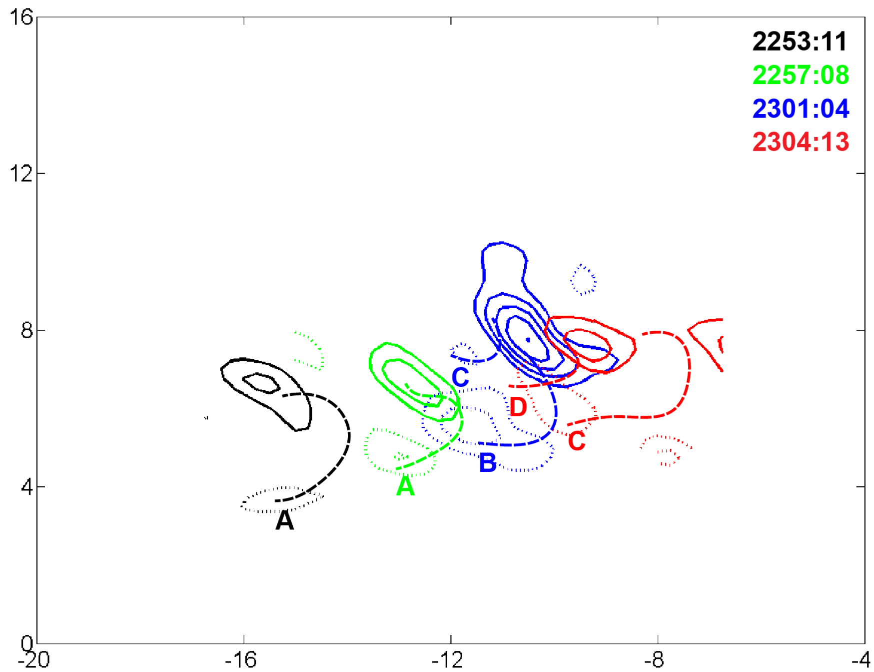

Fig. 5. Contours of objectively analyzed MWR-05XP 500 m azimuthal wind shear overlain with subjectively analyzed position of internal RFD surge gust fronts from TTUKa-2 radial velocity observations at (black) 2253:11, (green) 2257:08, (blue) 2301:04 and (red) 2304:13. Cyclonic azimuthal wind shear values (solid lines) are contoured every 0.005 s^{-1} starting with 0.01 s^{-1}, anticyclonic azimuthal wind shear values (dotted lines) are contoured every -0.005 s^{-1} starting with -0.005 s^{-1}. Analyzed internal RFD surge gust front positions are denoted by dashed lines and labeled as in Fig. 7. Axes are labeled in km from location of MWR-05XP.

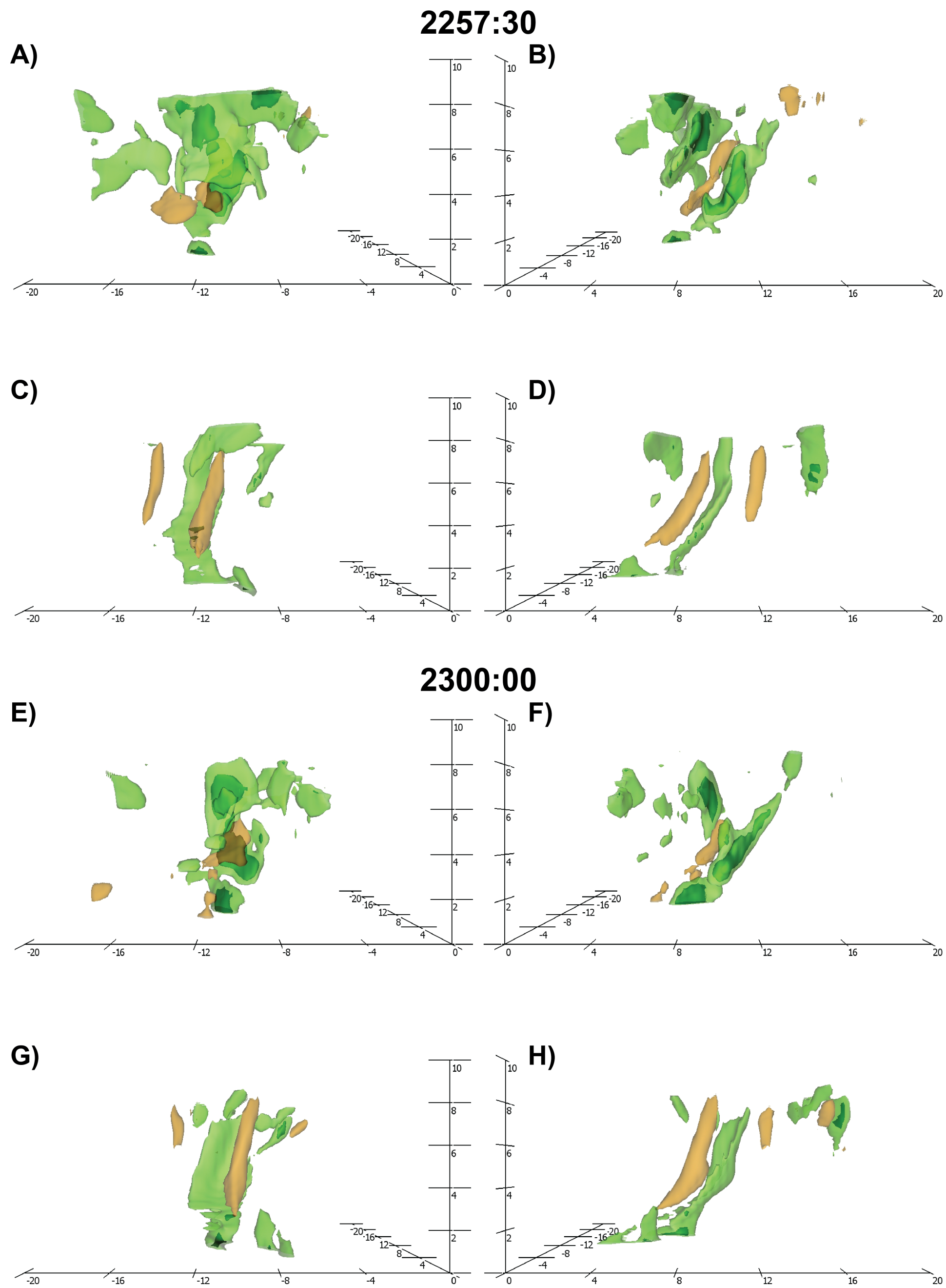

Fig. 6. Three-dimensional isosurfaces of MWR-05XP objectively analyzed azimuthal wind shear (A, B, E, F) and isosurfaces of EnKF ensemble mean vertical vorticity (C, D, G, H) at (A-D) 2257:30 and (E-H) 2300:00. Isosurfaces of 0.01(0.02), 0.015(0.03) and -0.01(-0.02) s^{-1} are plotted for azimuthal wind shear(vertical vorticity) in light green, dark green and brown, respectively. Perspective is from the south in A, C, E and G and from the east in B, D, F and H. MWR-05XP data are objectively analyzed to a grid with 500(250) m horizontal(vertical) spacing to correspond to the EnKF output.

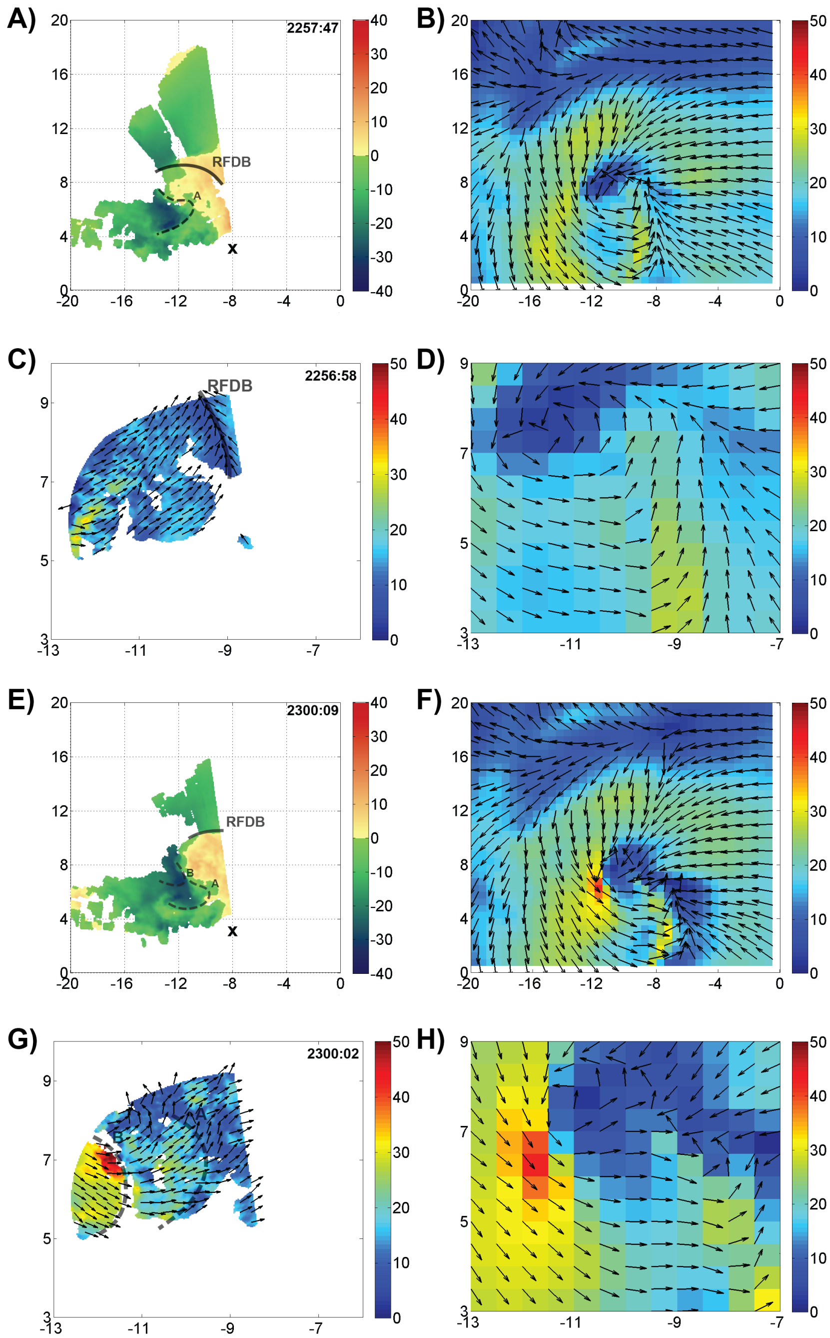

FIG. 7. (A, E) Objectively analyzed radial velocity data from TTUKa-2 (m s^{-1}), (C, G) TTUKa dual-Doppler synthesized wind vectors (m s^{-1}), (B, D, F, H) EnKF posterior ensemble mean wind vectors at the lowest vertical level (m s^{-1}). EnKF analyses are at (B, D) 2257:30 and (F, H) 2300:00. Axes are labeled in km from location of MWR-05XP deployment.